Fusion of hyperspectral and multispectral infrared astronomical images

Claire Guilloteau, Thomas Oberlin, Olivier Berné, Nicolas Dobigeon

Fusion of hyperspectral and multispectral infrared astronomical images

Claire Guilloteau
University of Toulouse
IRIT/INP-ENSEEIHT
Toulouse, France
claire.guilloteau@enseeiht.fr

Thomas Oberlin
University of Toulouse
ISAE-SUPAERO
Toulouse, France
thomas.oberlin@isae-supaero.fr

Olivier Berné
University of Toulouse
IRAP
Toulouse, France
olivier.berne@irap.omp.eu

Nicolas Dobigeon
University of Toulouse
IRIT/INP-ENSEEIHT
Toulouse, France
nicolas.dobigeon@enseeiht.fr

Abstract—This paper presents a data fusion method dedicated to high dimensional astronomical imaging. The fusion process reconstructs a high spatio-spectral resolution datacube, taking advantage of a multispectral observation image with high spatial resolution and a hyperspectral image with high spectral resolution. We define a regularized inverse problem accounting for the specificities of the astronomical observation instruments, in particular spectrally variant blurs. To handle convolution operators as well as the high dimensionality of the data, the problem is solved in the frequency domain and in a low-dimensional subspace. The fusion model is evaluated on simulated observations of the Orion Bar and shows excellent spatial and spectral reconstructions of the observed scene.

Index Terms—Data fusion, hyperspectral imaging, high dimensional imaging, astrophysics, super-resolution, spectrally varying blur.

I. INTRODUCTION

In the past two decades, the fusion of hyperspectral (HS) and multispectral (MS) images has become a common technique to provide a whole data-cube describing the acquired scene with high spatial *and* spectral resolutions. The fusion task aims at combining the high spectral resolution of the HS image with the high spatial resolution of the MS image. Such full resolution images find applications in remote sensing [1], planetology [2], material science [3], etc. In astrophysics, fused hyperspectral observations allow to derive, at a high spatial resolution, integrated maps of features (recombination lines, ions) unavailable in the MS data. In addition, maps of local physical conditions combining several spectral lines can be constructed with high angular resolution.

The data fusion problem has been traditionally investigated to combine MS and panchromatic (PAN) images for Earth observation [4]. The first methods emerged as heuristic approaches, e.g., based on component substitution [5], [6]. These fusion algorithms are fast and easy to implement and recover spatial details with high accuracy but are likely to produce important spectral distortions. The HS and MS images fusion problem led to new paradigms based on spectral unmixing and low-rank approximations of the data. These methods may also rely on observation forward models accounting for linear spectral degradations and spectrally constant spatial blur. In [7], [8], images are linearly decomposed into elementary spectra and spatial coefficients, following a non-negative matrix factorization (NMF) [9]. The fused product is formed by combining source spectra matrix from the HS image and the spatial components matrix extracted from the MS image. More recently, the fusion problem has been reformulated as an inverse problem complemented by spatial and/or spectral regularizations [10]–[12]. These methods also assume a low rank spectral approximation but they fully exploit the knowledge on the observation instruments.

In this paper, we propose a MS/HS image fusion method dedicated to astronomical images. We formulate a regularized inverse problem derived from the HS and MS observation forward models taking into consideration a spectrally variant blur. Indeed, the spatial resolution of spaceborne Earth observation images is limited by atmosphere turbulence [13] whereas the spatial resolution of spaceborne astronomical images is wavelength-dependent and limited by diffraction [14], [15]. This limit can be estimated by the Rayleigh criterion [16] which defines the angular resolution $\theta = 1.220\frac{\lambda}{D}$, where λ is the wavelength of the light and D the diameter of the aperture. To deal with the complexity significantly increased by this issue as well as the huge dimensionality of the data, we also propose a fast implementation suitable to fuse large astronomical datasets. The implementation relies on a reformulation in the Fourier domain and a resolution in a low-dimensional subspace, which significantly decreases the computational complexity.

The paper is organized as follows. Section II formulates the fusion inverse problem derived from the observational forward models. Section III introduces the proposed fast implementation. We perform the fusion task on a realistic simulated dataset of the Orion bar and assess the performance in Section IV. Conclusions are finally reported in Section V.

II. PROBLEM STATEMENT

The MS and HS images can be modeled through spectral and spatial degradations of a full resolution data-cube $\mathbf{X} \in$

$\mathbb{R}^{l_{\mathrm{h}} \times p_{\mathrm{m}}}$ we aim to recover. The forward models associated to those degradation processes can be written

$$\mathbf{Y}_{\mathrm{m}} = \mathbf{L}_{\mathrm{m}} \mathcal{M}(\mathbf{X}) + \mathbf{N}_{\mathrm{m}} \tag{1}$$

$$\mathbf{Y}_{\mathrm{h}} = \mathbf{L}_{\mathrm{h}} \mathcal{H}(\mathbf{X})\mathbf{S} + \mathbf{N}_{\mathrm{h}} \tag{2}$$

where $\mathbf{Y}_{\mathrm{m}} \in \mathbb{R}^{l_{\mathrm{m}} \times p_{\mathrm{m}}}$ and $\mathbf{Y}_{\mathrm{h}} \in \mathbb{R}^{l_{\mathrm{h}} \times p_{\mathrm{h}}}$ are respectively the MS and HS observed images, $l.$ and $p.$ denote the numbers of spectral bands and pixels, respectively, with $l_{\mathrm{m}} < l_{\mathrm{h}}$ and $p_{\mathrm{h}} < p_{\mathrm{m}}$. The spectral degradation operators $\mathbf{L}_{\mathrm{m}} \in \mathbb{R}^{l_{\mathrm{m}} \times l_{\mathrm{h}}}$ and $\mathbf{L}_{\mathrm{h}} \in \mathbb{R}^{l_{\mathrm{h}} \times l_{\mathrm{h}}}$ stand for the spectral response of each instrument. The spatial degradation operators $\mathcal{M} : \mathbb{R}^{l_{\mathrm{h}} \times p_{\mathrm{m}}} \to \mathbb{R}^{l_{\mathrm{h}} \times p_{\mathrm{m}}}$ in (1) and $\mathcal{H} : \mathbb{R}^{l_{\mathrm{h}} \times p_{\mathrm{m}}} \to \mathbb{R}^{l_{\mathrm{h}} \times p_{\mathrm{m}}}$ in (2) are 2-D spatial convolutions with spectrally variant kernels and model the blurs caused by the optical systems. This blur is linearly dependent of the wavelength, following a Rayleigh criterion [16]. The matrix $\mathbf{S} \in \mathbb{R}^{p_{\mathrm{m}} \times p_{\mathrm{h}}}$ is a downsampling operator with an integer decimation factor d such that $p_{\mathrm{h}} = \frac{p_{\mathrm{m}}}{d^2}$. Finally $\mathbf{N}_{\mathrm{m}}$ and $\mathbf{N}_{\mathrm{h}}$ stand for random noise and model mismodeling.

Recovering $\mathbf{X}$ from these two observations $\mathbf{Y}_{\mathrm{m}}$ and $\mathbf{Y}_{\mathrm{h}}$ can be formulated as the generic optimization problem

$$\hat{\mathbf{X}} = \underset{\mathbf{X}}{\operatorname{argmin}} \left(\frac{1}{2\sigma_{\mathrm{m}}^2} \|\mathbf{Y}_{\mathrm{m}} - \mathbf{L}_{\mathrm{m}} \mathcal{M}(\mathbf{X})\|_{\mathrm{F}}^2 \right.$$
$$\left. + \frac{1}{2\sigma_{\mathrm{h}}^2} \|\mathbf{Y}_{\mathrm{h}} - \mathbf{L}_{\mathrm{h}} \mathcal{H}(\mathbf{X})\mathbf{S}\|_{\mathrm{F}}^2 + \varphi_{\mathrm{spec}}(\mathbf{X}) + \varphi_{\mathrm{spac}}(\mathbf{X}) \right) \tag{3}$$

where the two first terms are related to MS and HS observations, generally named as data fidelity terms. The two last terms $\varphi_{\mathrm{spec}}(\cdot)$ and $\varphi_{\mathrm{spac}}(\cdot)$ are spectral and spatial regularization terms discussed hereafter. First, the pixel spectra of $\mathbf{X}$ are expected to live in a subspace whose dimension l_{sub} is much smaller than the spectral dimension l_{h} [10], [11], [17]. This can be formulated by rewriting $\mathbf{X} = \mathbf{VZ}$, where the matrix $\mathbf{Z} \in \mathbb{R}^{l_{\mathrm{sub}} \times p_{\mathrm{m}}}$ is the projection of $\mathbf{X}$ onto the subspace spanned by $\mathbf{V} \in \mathbb{R}^{l_{\mathrm{h}} \times l_{\mathrm{sub}}}$, which gathers elementary spectra. Imposing this low-rank structure implicitly ensures a spectral regularization. The spectra composing the columns of $\mathbf{V}$ are generally identified beforehand, e.g., by a principal component analysis (PCA) of the HS image. Furthermore, we define $\varphi_{\mathrm{spac}}(\cdot)$ based on a Sobolev regularization, assuming that the image to be reconstructed is *a priori* spatially smooth.

$$\varphi_{\mathrm{spac}}(\mathbf{Z}) = \mu \|\mathbf{ZD}\|_{\mathrm{F}}^2$$

where $\mathbf{D}$ is a 1st order 2-D finite differences operator and $\mu \geq 0$ is the regularization parameter adjusting the strength of the regularization.

III. FAST IMPLEMENTATION

A. Reformulation in the Fourier domain

In high dimensional imaging, spectrally variant kernels in $\mathcal{M}(\cdot)$ and $\mathcal{H}(\cdot)$ prevent an efficient direct application of fast gradient descent [18] or conjugate gradient [19]. Indeed, evaluating the gradient at each iteration requires computing thousands of convolutions and on-the-fly loading of each point spread function (PSF), leading to a considerable computational complexity both in time and memory.

First, we fully reformulate the problem in the Fourier domain. We denote by $\odot$ the element-wise matrix multiplication and $\mathbf{F}$ the 2D discrete Fourier transform matrix ($\mathbf{FF}^H = \mathbf{F}^H\mathbf{F} = \mathbf{I}$) such that $\dot{\mathbf{Z}} = \mathbf{ZF}$, $\dot{\mathbf{Y}}_{\mathrm{m}} = \mathbf{Y}_{\mathrm{m}}\mathbf{F}$ and $\dot{\mathbf{Y}}_{\mathrm{h}} = \mathbf{Y}_{\mathrm{h}}\mathbf{F}$. Under periodic boundary assumptions, the spectrally variant convolutions $\mathcal{M}(\cdot)$ and $\mathcal{H}(\cdot)$ are rewritten as point-wise multiplications, such that, for any spectral band l

$$(\mathcal{M}(\mathbf{VZ}))^l \simeq \left(\dot{\mathbf{M}}^l \odot (\mathbf{V}\dot{\mathbf{Z}})^l \right) \mathbf{F}^H$$

$$(\mathcal{H}(\mathbf{VZ}))^l \simeq \left(\dot{\mathbf{H}}^l \odot (\mathbf{V}\dot{\mathbf{Z}})^l \right) \mathbf{F}^H$$

where $\dot{\mathbf{M}}^l$ and $\dot{\mathbf{H}}^l$ stand for the 2-D discrete Fourier transforms (DFT) of the PSFs related to the multi- and the hyperspectral observation instruments, respectively. Then, the subsampling operator $\mathbf{S}$ is written in the Fourier domain as an aliasing operator $\dot{\mathbf{S}} = \mathbf{SF}$, which sums d^2 equally weighted blocks of an input matrix. This operator acts independently on every p_{m} pixels spectral band to produce a $p_{\mathrm{h}} = \frac{p_{\mathrm{m}}}{d}$ pixels output. The spatial regularization term can also be expressed in the Fourier domain, as the operator $\mathbf{D}$ can be seen as a 2D convolution operator with kernels $\begin{pmatrix} 1 & -1 \end{pmatrix}$ and $\begin{pmatrix} 1 \\ -1 \end{pmatrix}$. Under cyclic boundary conditions, we express the regularization term as a point-wise multiplication such that

$$\mathbf{ZD} = \left(\dot{\mathbf{Z}} \odot \dot{\mathbf{D}} \right) \mathbf{F}^H.$$

Following Parseval's identity, the problem (3) is rewritten

$$\hat{\dot{\mathbf{Z}}} = \underset{\dot{\mathbf{Z}}}{\operatorname{argmin}} \left(\frac{1}{2\sigma_{\mathrm{m}}^2} \|\dot{\mathbf{Y}}_{\mathrm{m}} - \mathbf{L}_{\mathrm{m}}((\mathbf{V}\dot{\mathbf{Z}}) \odot \dot{\mathbf{M}})\|_{\mathrm{F}}^2 \right.$$
$$\left. + \frac{1}{2\sigma_{\mathrm{h}}^2} \|\dot{\mathbf{Y}}_{\mathrm{h}} - \mathbf{L}_{\mathrm{h}}((\mathbf{V}\dot{\mathbf{Z}}) \odot \dot{\mathbf{H}})\dot{\mathbf{S}}\|_{\mathrm{F}}^2 + \mu\|\dot{\mathbf{Z}} \odot \dot{\mathbf{D}}\|_{\mathrm{F}}^2 \right). \tag{4}$$

Finally, the fused product is then obtained by $\hat{\mathbf{X}} = \mathbf{V}\hat{\dot{\mathbf{Z}}}\mathbf{F}^H$.

B. Vectorization

Subsequently, we propose to solve the problem in the low-dimensional subspace spanned by the columns of $\mathbf{V}$ after vectorizing all quantities with the dedicated notations

$$\dot{\mathbf{y}}_{\mathrm{m}} = \left[\dot{\mathbf{Y}}_{\mathrm{m}}^1 \ldots \dot{\mathbf{Y}}_{\mathrm{m}}^{l_{\mathrm{m}}} \right]^T \qquad \dot{\mathbf{y}}_{\mathrm{h}} = \left[\dot{\mathbf{Y}}_{\mathrm{h}}^1 \ldots \dot{\mathbf{Y}}_{\mathrm{h}}^{l_{\mathrm{h}}} \right]^T$$

$$\underline{\mathbf{V}} = \mathbf{V} \otimes \mathbf{I}_{p_{\mathrm{m}} \times p_{\mathrm{m}}} \qquad \dot{\mathbf{z}} = \left[\dot{\mathbf{Z}}^1 \ldots \dot{\mathbf{Z}}^{l_{\mathrm{sub}}} \right]^T$$

where $\otimes$ stands for the Kronecker product and $\mathbf{I}_{p \times q}$ the $p \times q$ identity matrix. Hereafter, we denote by $\underline{\mathbf{L}}_{\mathrm{m}}$, $\underline{\mathbf{L}}_{\mathrm{h}}$, $\underline{\dot{\mathbf{M}}}$, $\underline{\dot{\mathbf{H}}}$, $\underline{\dot{\mathbf{S}}}$ and $\underline{\dot{\mathbf{D}}}$ the vectorized forms of $\mathbf{L}_{\mathrm{m}}$, $\mathbf{L}_{\mathrm{h}}$, $\dot{\mathbf{M}}$, $\dot{\mathbf{H}}$, $\dot{\mathbf{S}}$ and $\dot{\mathbf{D}}$, respectively, such that

$$\underline{\mathbf{L}}_{\mathrm{m}}\underline{\dot{\mathbf{M}}}\underline{\mathbf{V}}\dot{\mathbf{z}} = \begin{bmatrix} \left[\mathbf{L}_{\mathrm{m}}((\mathbf{V}\dot{\mathbf{Z}}) \odot \dot{\mathbf{M}}) \right]^1 \\ \vdots \\ \left[\mathbf{L}_{\mathrm{m}}((\mathbf{V}\dot{\mathbf{Z}}) \odot \dot{\mathbf{M}}) \right]^{l_{\mathrm{m}}} \end{bmatrix}$$

and

$$\underline{\dot{\mathbf{S}}}\mathbf{L}_{\mathrm{h}}\dot{\mathbf{H}}\mathbf{V}\dot{\mathbf{z}} = \begin{bmatrix} \left[\mathbf{L}_{\mathrm{h}}((\mathbf{V}\dot{\mathbf{Z}}) \odot \dot{\mathbf{H}})\dot{\mathbf{S}} \right]^1 \\ \vdots \\ \left[\mathbf{L}_{\mathrm{h}}((\mathbf{V}\dot{\mathbf{Z}}) \odot \dot{\mathbf{H}})\dot{\mathbf{S}} \right]^{l_{\mathrm{h}}} \end{bmatrix}.$$

Using these notations, setting the gradient in (4) to zero amounts to solving the following linear system

$$\mathbf{A}\dot{\mathbf{z}} = \mathbf{b} \tag{5}$$

where $\mathbf{A} \in \mathbb{R}^{l_{\mathrm{sub}}p_{\mathrm{m}} \times l_{\mathrm{sub}}p_{\mathrm{m}}}$ and $\mathbf{b} \in \mathbb{R}^{l_{\mathrm{sub}}p_{\mathrm{m}}}$ are defined

$$\mathbf{A} = \frac{1}{\sigma_{\mathrm{m}}^2}\underline{\mathbf{V}}^H\dot{\underline{\mathbf{M}}}^H\mathbf{L}_{\mathrm{m}}^H\mathbf{L}_{\mathrm{m}}\dot{\mathbf{M}}\mathbf{V}$$
$$+ \frac{1}{\sigma_{\mathrm{h}}^2}\underline{\mathbf{V}}^H\dot{\underline{\mathbf{H}}}^H\underline{\mathbf{L}}_{\mathrm{h}}^H\dot{\underline{\mathbf{S}}}^H\underline{\dot{\mathbf{S}}}\mathbf{L}_{\mathrm{h}}\dot{\mathbf{H}}\mathbf{V} + \mu\dot{\underline{\mathbf{D}}}^H\dot{\mathbf{D}}, \tag{6}$$

$$\mathbf{b} = -\frac{1}{\sigma_{\mathrm{m}}^2}\underline{\mathbf{V}}^H\dot{\underline{\mathbf{M}}}^H\mathbf{L}_{\mathrm{m}}^H\dot{\mathbf{y}}_{\mathrm{m}} - \frac{1}{\sigma_{\mathrm{h}}^2}\underline{\mathbf{V}}^H\dot{\underline{\mathbf{H}}}^H\underline{\mathbf{L}}_{\mathrm{h}}^H\dot{\underline{\mathbf{S}}}^H\dot{\mathbf{y}}_{\mathrm{h}}. \tag{7}$$

These quantities $\mathbf{A}$ and $\mathbf{b}$ combine all spatial and spectral operators to be expressed in the low-dimensional subspace. As explicitly written in (6), the backward and forward projection operators $\underline{\mathbf{V}}$ and $\underline{\mathbf{V}}^H$ gathered in $\mathbf{A}$ enable the wavelength-dependent PSFs in $\dot{\mathbf{M}}$ and $\dot{\mathbf{H}}$ to be combined. Furthermore, this matrix $\mathbf{A}$ is symmetric and sparse, composed of $d^2 l_{\mathrm{sub}}^2 p_{\mathrm{m}}$ non-zero over $l_{\mathrm{sub}}^2 p_{\mathrm{m}}^2$ entries. Consequently, the matrix $\mathbf{A}$ can be computed only once as a pre-processing step and stored in memory at low cost. An efficient computing scheme of this sparse matrix is detailed in [20]. Afterwards, the problem (5) can be solved with a gradient-based algorithm [18], [19] by calling this matrix $\mathbf{A}$ along iterations, significantly decreasing the computational complexity in terms of time and memory.

IV. EXPERIMENTS

A. Synthetic data

In this section, we study the performance of the proposed fast fusion method on a realistic simulated dataset of the Orion Bar. This dataset has been generated to assess data fusion performed on high dimensional astronomical observations [21]. It is composed of a simulated reference image of high spatial and high spectral resolution and corresponding HS and MS images that would be observed by two dedicated sensors. The simulated scene represents a photodissociation region (PDR) located in the Orion Bar and is built under a low-rank assumption. More precisely, this simulated PDR is a linear combination of 4 elementary spectra and 4 spatial maps derived from real observations. This reference image is composed of 300×300 pixels and 4974 spectral bands in the near-infrared range, from 1 to 2.35 microns. A RGB composition of 3 spectral lines of this image is shown in Fig. 2 a).

From this reference scene, MS and HS observed images have been derived following forward models (1) and (2) to mimic observations of the near-infrared camera (NIRCam) imager and the near-infrared spectrograph integral field unit (NIRSpec IFU) embedded in the James Webb Space Telescope
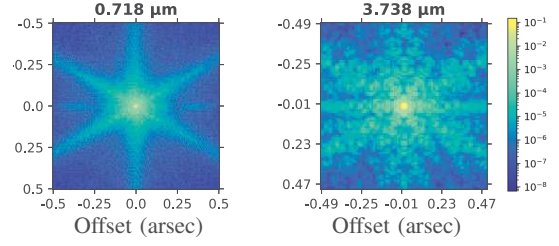

Fig. 1. PSFs of the NIRCam Imager calculated with *webbpsf* [26] for two particular wavelengths (logarithmic scale).

(JWST) [22]. The MS image is composed of 300×300 pixels and 11 spectral bands while the HS image is made of 100×100 pixels and 4974 spectral bands. The degradation operators that model the response of the two instruments are provided by the JWST documentation [23]–[25]. Figure 1 emphasizes the spectral dependency of the PSFs of the NIRCam Imager.

To mimic a mixed Poisson-Gaussian noise, the noise-free measurements are first corrupted by a multiplicative Gaussian noise of mean and variance the photon count in the pixel. Then we consider an additive spatially correlated Gaussian noise whose mean and covariance depend on the instruments, as specified in the JWST documentation. To evaluate the performance of our method on low SNR observations, we consider that the signal is 10 times less intense than the expected signal that would be observed in the Orion bar region presented in [21]. MS and HS observed images are shown in Fig. 2 b) and c) as RGB compositions of 3 spectral bands.

B. Compared methods

First, we compare our fusion algorithm with a naive super-resolution technique, hereafter referred to as the baseline method. As for the proposed method, it relies on a low-rank assumption on the spectral content and consists in up-sampling the projection of the HS image onto the spectral signal subspace with a bi-cubic spline interpolation. Secondly, we consider the Brovey method which has been intensively used for fusing MS and PAN images in the context of Earth observation. It consists in extracting spatial details from the MS image that are subsequently injected into an up-sampled interpolated version of the projection of the HS image onto the spectral subspace [27]. Finally, we evaluate the two non-symmetric counterparts of our method derived from the original inverse problem (3). The first one, called MS-only, considers a unique data fitting term associated with the MS image in (3). Thus, this problem is equivalent to the spectral reconstruction of the MS image, similarly to [28]. The second one, HS-only, can be seen as a hyperspectral super-resolution method as only the data fitting term related to the HS image is kept. Note that all aforementioned methods, as well as the proposed one, require a spectral subspace identification. In this work, this step has been performed by a PCA on the HS image.
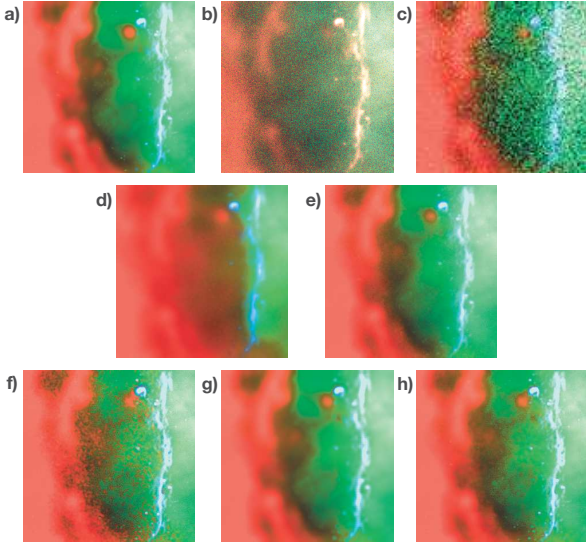
Fig. 2. RGB compositions of a) the reference image, b) the multispectral observed image, c) the hyperspectral observed image and fused products of d) the baseline, e) the Brovey, f) the MS-only, g) the HS-only and h) the proposed methods.
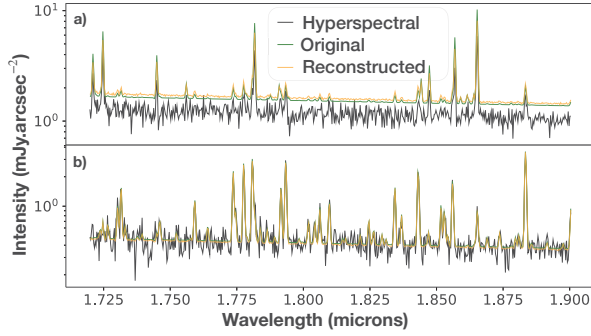

Fig. 3. Hyperspectral, reference and reconstructed (with the proposed method) spectra from a) a sharp edge and b) a smooth region corresponding to a pixel displayed in blue and red respectively in Fig. 2.

C. Results

Figure 2 d) to h) shows RGB compositions of the fused products along with the reference image (a) to reconstruct. The proposed method clearly provides the best visual results. In particular, the reconstruction of thin spatial details around edges (blue pixels) appears to be much better than the baseline, Brovey and HS-only results. The MS-only method seems able to reconstruct these details but produces a noisier fused image. Spectra of the hyperspectral image, reference image and reconstructed image with the proposed method are presented in Fig. 3 for two particular areas. On the top (resp. bottom), the spectra are associated to a pixel in a sharp (resp. smooth) region, displayed in blue (resp. red) in Fig 2. For the two regions, our method is able to recover most of the lines, even of low-intensity. More generally, the spectral reconstruction

Methods	aSAM	aSSIM	PSNR	Time
Baseline	0.052	0.9502	66.90	/
Brovey	0.052	**0.9930**	69.48	19
HS-only	**0.029**	0.9741	**70.69**	1300 + 20
MS-only	0.068	0.9908	70.38	600 + 15
Proposed	**0.037**	**0.9948**	**72.64**	1900 + 20

is excellent but Fig. 3 a) underlines the limitations of the spatial regularization which smooths intensities around sharp edges and leads to spectral aberrations. According to these two illustrations, the spatial and spectral denoising performed by the fusion seems to be efficient.

To evaluate the quality of the reconstruction beyond a crude visual inspection, we propose to study three quantitative measures. We assess the quality of the spectral reconstruction by computing the spectral angle mapper (SAM) [29]. This value measures the spectral distortion between the reference and reconstructed spectra. Here, we denote aSAM the average SAM values over the pixels. Then, we consider the structural similarity (SSIM) index [30], evaluating the degradation of spatial structures on each spectral band. We rather calculate its average value denoted aSSIM across all bands. Finally, the peak signal-to-noise ratio (PSNR) is used to evaluate the overall reconstruction quality in the least-square sense. A low value of aSAM as well as a close to 1 aSSIM value and a large PSNR indicate a good reconstruction. The quantitative results are reported in Table I where, for each metric, the two best results appear in bold. Compared to all the other methods, the proposed fusion algorithm appears to be the best trade-off providing the best spatial and global reconstruction and the second best spectral reconstruction. While HS-only shows good spectral reconstruction but poor spatial results and the opposite for MS-only, the Brovey method only slightly improves the baseline reconstruction.

V. CONCLUSION

In this paper, we proposed a hyperspectral and multispectral image fusion method suitable to combine high dimensional astronomical images. We formulated observation forward models based on accurate instrumental properties and taking into account some specificities, in particular spectrally variant blurs. To solve this problem in a computationally efficient scheme, we introduced a fast implementation of the fusion task, capitalizing on the frequency properties of convolutions and on a low-rank assumption on the spectral content. Finally, we applied our fusion method to a simulated yet realistic scene of the Orion Bar and showed that it outperforms state-of-the-art methods, recovering spatial and spectral features. Future work includes the design of a tailored regularization and exhaustive tests on real data.

REFERENCES

[1] C.-I Chang, *Hyperspectral Data Exploitation: theory and applications.* Hoboken, NJ: John Wiley & Sons, 2007.

[2] S. Douté, B. Schmitt, Y. Langevin, J.-P. Bibring, F. Altieri, G. Bellucci, B. Gondet, F. Poulet, and the MEX OMEGA team, "South Pole of Mars: Nature and composition of the icy terrains from Mars Express OMEGA observations," *Planetary and Space Science*, vol. 55, pp. 113–133, Jan. 2007.

[3] C. Colliex, M. Tencé, E. Lefèvre, C. Mory, H. Gu, D. Bouchet, and C. Jeanguillaume, "Electron energy loss spectrometry mapping," *Microchimica Acta*, vol. 114, pp. 71–87, 1994.

[4] L. Loncan, L. B. de Almeida, J. M. Bioucas-Dias, X. Briottet, J. Chanussot, N. Dobigeon, S. Fabre, W. Liao, G. A. Licciardi, M. Simões, J. Tourneret, M. A. Veganzones, G. Vivone, Q. Wei, and N. Yokoya, "Hyperspectral pansharpening: A review," *IEEE Geoscience and Remote Sensing Magazine*, vol. 3, no. 3, pp. 27–46, Sep. 2015.

[5] G. Vivone, L. Alparone, J. Chanussot, M. Dalla Mura, A. Garzelli, G. A. Licciardi, R. Restaino, and L. Wald, "A Critical Comparison Among Pansharpening Algorithms," *IEEE Trans. Geosci. Remote Sens.*, vol. 53, no. 5, pp. 2565–2586, May 2015.

[6] A. R. Gillespie, A. B. Kahle, and R. E. Walker, "Color enhancement of highly correlated images. II. Channel ratio and "chromaticity" transformation techniques," *Remote Sensing of Environment*, vol. 22, no. 3, pp. 343–365, Aug 1987.

[7] O. Berné, A. Helens, P. Pilleri, and C. Joblin, "Non-negative matrix factorization pansharpening of hyperspectral data: An application to mid-infrared astronomy," in *Proc. IEEE GRSS Workshop Hyperspectral Image SIgnal Process.: Evolution in Remote Sens. (WHISPERS)*, 06 2010, pp. 1–4.

[8] N. Yokoya, T. Yairi, and A. Iwasaki, "Coupled Nonnegative Matrix Factorization Unmixing for Hyperspectral and Multispectral Data Fusion," *IEEE Trans. Geosci. Remote Sens.*, vol. 50, no. 2, pp. 528–537, Feb 2012.

[9] D. D. Lee and H. S. Seung, "Learning the parts of objects by non-negative matrix factorization," *Nature*, vol. 401, no. 6755, pp. 788–791, Oct 1999.

[10] M. Simoes, J. Bioucas-Dias, L. B. Almeida, and J. Chanussot, "A Convex Formulation for Hyperspectral Image Superresolution via Subspace-Based Regularization," *IEEE Trans. Geosci. Remote Sens.*, vol. 53, no. 6, pp. 3373–3388, Jun 2015.

[11] Q. Wei, N. Dobigeon, and J.-Y. Tourneret, "Fast Fusion of Multi-Band Images Based on Solving a Sylvester Equation," *IEEE Trans. Image Process.*, vol. 24, no. 11, pp. 4109–4121, Nov 2015.

[12] Q. Wei, J. Bioucas-Dias, N. Dobigeon, and J.-Y. Tourneret, "Hyperspectral and multispectral image fusion based on a sparse representation," *IEEE Trans. Geosci. Remote Sens.*, vol. 53, no. 7, pp. 3658–3668, Jul 2015.

[13] J. E. Pearson, "Atmospheric turbulence compensation using coherent optical adaptive techniques," *Appl. Opt.*, vol. 15, no. 3, pp. 622–631, Mar 1976.

[14] F. Soulez, E. Thiébaut, and L. Denis, "Restoration of Hyperspectral Astronomical Data with Spectrally Varying Blur," in *EAS Publications Series*, ser. EAS Publications Series, D. Mary, C. Theys, and C. Aime, Eds., vol. 59, Mar 2013, pp. 403–416.

[15] M. A. Hadj-Youcef, F. Orieux, A. Fraysse, and A. Abergel, "Restoration from multispectral blurred data with non-stationary instrument response," in *Proc. European Signal Process. Conf. (EUSIPCO)*, Aug 2017, pp. 503–507.

[16] L. Rayleigh, "Investigations in optics, with special reference to the spectroscope," *Monthly Notices of the Royal Astronomical Society : Letters*, vol. 40, p. 254, Feb 1880.

[17] E. Wycoff, T.-H. Chan, K. Jia, W.-K. Ma, and Y. Ma, "Non-negative sparse promoting algorithm for high resolution hyperspectral imaging," in *Proc. IEEE Int. Conf. Acoust., Speech and Signal Process. (ICASSP)*, Vancouver, Canada, 2013.

[18] A. Beck and M. Teboulle, "A fast iterative shrinkage-thresholding algorithm for linear inverse problems," *SIAM J. Imaging Sciences*, vol. 2, pp. 183–202, 01 2009.

[19] J. R. Shewchuk, "An introduction to the conjugate gradient method without the agonizing pain," Pittsburgh, PA, USA, Tech. Rep., 1994.

[20] C. Guilloteau, T. Oberlin, O. Berné, and N. Dobigeon, "Hyperspectral and multispectral image fusion under spectrally varying spatial blurs – Application to high dimensional infrared astronomical imaging," *arXiv preprint*, Dec. 2019. [Online]. Available: https://arxiv.org/abs/1912.11868/

[21] C. Guilloteau, T. Oberlin, O. Berné, É. Habart, and N. Dobigeon, "Simulated JWST datasets for multispectral and hyperspectral image fusion," *arXiv preprint*, Jan. 2020. [Online]. Available: https://arxiv.org/abs/2001.02618/

[22] J. P. Gardner, J. C. Mather, M. Clampin, R. Doyon, M. A. Greenhouse, H. B. Hammel, J. B. Hutchings, P. Jakobsen, S. J. Lilly, and K. S. Long, "The James Webb Space Telescope," *Space Science Reviews*, vol. 123, no. 4, pp. 485–606, Apr 2006.

[23] Space Telescope Science Institute (STScI), *NIRCam Filters, JWST User Documentation [Published 2017 November 29]*, Baltimore, MD, 2017. [Online]. Available: https://jwst-docs.stsci.edu/near-infrared-camera/nircam-instrumentation/nircam-filters

[24] ——, *NIRSpec Integral Field Unit, JWST User Documentation [Published 2017 March 29]*, Baltimore, MD, 2017. [Online]. Available: https://jwst-docs.stsci.edu/near-infrared-spectrograph/nirspec-instrumentation/nirspec-integral-field-unit

[25] ——, *NIRSpec Dispersers and Filters, JWST User Documentation [Published 2017 March 29]*, Baltimore, MD, 2017. [Online]. Available: https://jwst-docs.stsci.edu/near-infrared-spectrograph/nirspec-instrumentation/nirspec-dispersers-and-filters

[26] M. D. Perrin, R. Soummer, E. M. Elliott, M. D. Lallo, and A. Sivaramakrishnan, "Simulating point spread functions for the James Webb Space Telescope with WebbPSF," in *Space Telescopes and Instrumentation 2012: Optical, Infrared, and Millimeter Wave*, ser. Society of Photo-Optical Instrumentation Engineers (SPIE) Conference Series, vol. 8442, Sep 2012, p. 84423D.

[27] T.-M. Tu, S.-C. Su, H.-C. Shyu, and P. S. Huang, "A new look at ihs-like image fusion methods," *Information Fusion*, vol. 2, no. 3, pp. 177 – 186, 2001.

[28] M. e. A. Hadj-Youcef, F. Orieux, A. Fraysse, and A. Abergel, "Spatio-spectral multichannel reconstruction from few low-resolution multispectral data," in *Proc. European Signal Process. Conf. (EUSIPCO)*, Rome, Italy, Sept. 2018.

[29] F. A. Kruse, A. B. Lefkoff, J. W. Boardman, K. B. Heidebrecht, A. T. Shapiro, P. J. Barloon, and A. F. H. Goetz, "The spectral image processing system (sips)—interactive visualization and analysis of imaging spectrometer data," *Remote Sens. Environment*, vol. 44, no. 2-3, pp. 145–163, May 1993.

[30] Z. Wang, A. C. Bovik, H. R. Sheikh, and E. P. Simoncelli, "Image quality assessment: From error visibility to structural similarity," *IEEE Trans. Image Process.*, vol. 13, no. 4, pp. 600–612, Apr 2004.